RSC Advances

ROYAL SOCIETY
OF CHEMISTRY

www.rsc.org/advances

Graphene Stabilized High-κ Dielectric Y_2O_3 (111) Monolayer and Their Interfacial Properties

Ting Ting Song,[1] **Ming Yang,**[2] [†] **Martin Callsen,**[3] **Qing Yun Wu,**[3] **Jun Zhou,**[3] **Shao Feng Wang,**[1] **Shi Jie Wang,**[2]**and Yuan Ping Feng** [3] [‡]

The exfoliation of graphene triggers dramatic interest to explore other two-dimensional materials for functionalizing future nanoelectronic devices. In this study, *via* first-principles calculations, we predict a stable planar Y_2O_3 (111) monolayer with a direct band gap of 3.96 eV. This high-κ dielectric monolayer can be further stabilized by graphene substrate. The interaction between the planar Y_2O_3 (111) monolayer and graphene is found to be weak and dominated by van der Waals interaction, while the electronic properties are determined by orbital hybridization and electrostatic interaction. Our results indicate that high-κ dielectric monolayer can be formed on a substrate with weak interfacial interaction *via* physical deposition process, and shed light on engineering extremely thin high-κ dielectrics on graphene based electronics with desired properties.

[1] *Institute for Structure and Function and Department of Physics, Chongqing University, Chongqing, People's Republic of China 400044.*

[2] *Institute of Materials Research and Engineering, 3 Research Link, Singapore 117602.*

[3] *Department of Physics, National University of Singapore, 2 Science Drive 3, Singapore 117542.*

Correspondence and requests for materials should be addressed to M. Y[†] (e-mail: yangm@imre.a-star.edu.sg) or Y. P. F[‡] (e-mail: phyfyp@nus.edu.sg)

1 Introduction

In the past decades, the performance of silicon (Si) based field-effect transistors (FETs) has been improved dramatically by scaling technology. Due to the relative small dielectric constant of SiO_2, the thickness of this gate dielectric is now approaching its physical limit. In order to further improve the performance of FETs, high-κ dielectrics such as HfO_2 have replaced conventional gate dielectric SiO_2, due to its much larger dielectric constant. [1,2] On the other hand, tremendous effects have also been made to find a channel material with high carrier mobility to substitute Si, in which graphene, a monolayer of carbon atoms with honeycomb lattices, has been a focus in recent years. [3–5] Graphene has many fascinating mechanical, optical, and electronic properties. One of the interesting properties of graphene is the high intrinsic carrier mobility as it is highly desired for future high speed electronic devices. [6] It has been reported that the electron mobility of free standing graphene is up to 200,000 $cm^2 \cdot V^{-1} \cdot s^{-1}$ at room temperature. [7] Integrating high-κ dielectrics into graphene based electric devices takes advantages of both materials. The interface between graphene and high-κ oxide is expected to play a crucial role in the performance of such devices. [8] However, the graphene/high-κ dielectrics interface is different from that of Si/high-κ dielectrics interface, resulting from the inert surface of graphene. Extensive studies have been carried out to understand interfacial interaction between graphene and high-κ dielectrics. It is found that the interaction between graphene and high-κ dielectrics strongly depends on the surface chemical environment of the dielectrics. [9–14] Experimentally, various high-κ dielectrics have been grown on graphene, including HfO_2 [15], Al_2O_3 [8], ZrO_2 [16], Si_3N_4 [17–19], and Y_2O_3 [20,21] thin films or nanoribbons. The electric properties of these graphene/high-κ dielectric devices have been improved much compared to SiO_2 because high-κ dielectrics can increase capacitance density significantly and also screen the scattering of interfacial charged impurities effectively.

Following graphene, many other two-dimensional materials have been found, which include graphene like silicene, [22] h-BN, [3] transition metal dichalcogenides such as MoS_2 [3], black phosphorene [23,24], as well as III-V and II-VI materials. [25–30] More recently, crystalline double-layer SiO_2 sheet has been deposited on Ru(0001) substrate. [31] It is noted that when the thickness of dielectric thin films is reduced, the interaction between graphene and the dielectric might be changed accordingly. For example, for graphene adsorbed on the Al_2O_3 (0001) surface, the interaction between them is found strong [12], while in contrast, weak interaction is found at the interface between graphene and Y_2O_3 (111) monolayer [32]. In addition, graphene has been assembled on single layer of h-BN, and the interaction between them is dominated by van der Waals (vdW) force. [33] These results indicate that both surface chemical environment and the thickness of

dielectrics might play an important role in determining the interaction between graphene and the dielectrics, and motivate us to study the stability of high-κ oxide dielectric monolayer and its interfacial properties with graphene. In this study, based on first-principles calculation, we find that free standing planar Y_2O_3 (111) monolayer is stable, and its stability can be further enhanced when it is supported by graphene. In addition, the interfacial interaction between them is weak, with the main contribution arising from vdW interaction, while the electronic properties are mainly determined by electrostatic interaction and orbital hybridization between C p_z and O p_z, as well as C p_z and Y $4d$ orbitals.

2 Methodology

All calculations were carried out by using density-functional theory (DFT) as implemented in VASP code.[34,35] Generalized gradient approximation (GGA) in the form of Perdew-Burke-Ernzerhof (PBE) was used for the exchange-correlation functional, and the projector augmented wave (PAW) potentials were selected to describe the interaction between electrons and ions.[36] The cutoff energy for the plane wave expansion was set to 500 eV. Γ centered $18\times18\times1$ and $4\times4\times4$ κ-point meshes were used to sample the first Brillouin zone of pristine graphene and Y_2O_3 bulk, and $9\times9\times1$ κ-point meshes were applied for Y_2O_3 (111) monolayer, Y_2O_3 (111) monolayer on graphene, and Y_2O_3 (111) monolayer on Y (0001) surface, respectively. To minimize the interaction between image surfaces, 15 Å vacuum was applied normal to Y_2O_3 surface for all interface structures. Corrections for vdW effects were included in the calculations by using Grimme's DFT-D2 method with C_6 (1.75, 0.70, and 24.67) and R_0 (1.452, 1.342, and 1.639) for C, O, and Y atoms, respectively. The DFT-D2 calculation results were partially compared with the results by the self-consistent *ab initio* van der Waals density-functional (vdW-DF) method.[37,38] All structures were optimized until residual force on each atom is smaller than 0.01 eV/Å. For the electronic structure of Y_2O_3 monolayer, Heyd-Scuseria-Ernzerhof hybrid functionals (HSE06) have been used.[39] To examine thermal stability of Y_2O_3 (111) monolayer, *ab initio* molecular dynamics simulations were performed with a time step of 1 *fs*, canonical ensemble (NVT), and Nos*é* heat bath. In addition, phonon dispersion was calculated using density functional perturbation theory implemented in VASP with higher electronic convergence criterion of 10^{-8} eV and analyzed by using the PHONOPY code.[40] Based on these settings, the calculated lattice constant and PBE band gap of Y_2O_3 bulk are 10.51 Å and 4.5 eV, respectively, in good agreement with previous results.[41]

3   Results and Discussions

Clean Y_2O_3 (111) surface is polar, terminated by O atoms, which is unstable and structural relaxation or even reconstruction is needed to suppress surface polarization.[44] Especially when the thickness of Y_2O_3 (111) thin films approaches its physical limit one monolayer, the Y_2O_3 (111) single layer may undergo structural reconstruction. The reconstructed Y_2O_3 (111) monolayer shown in Fig. 1(a) is a hexagonal planar structure with 3 O atoms and 2 Y atoms in the unit cell with lattice constant of 7.22 Å. It is noted that the planar form is energetically most stable for Y_2O_3 (111) and its total energy is about 0.6 eV/atom lower than that of a buckled structure. The Y-O bond length in Y_2O_3 (111) monolayer is 2.08 Å, about 0.2 Å smaller than that in bulk Y_2O_3, indicating stronger in-plane bonding in monolayer Y_2O_3 due to reduced coordinations.[43] The suppression of surface polarization in this planar Y_2O_3 (111) monolayer also leads to enhanced in-plane covalent bonding character, because the calculated Bader charges suggest an ionic formula of $Y_2^{+1.95}O_3^{-1.3}$, less than $Y_2^{+2.16}O_3^{-1.44}$ in bulk form.[42] Figure. 1(b) is the calculated phonon spectra of the planar Y_2O_3 (111) monolayer. No imaginary frequency has been found, indicating that the planar Y_2O_3 (111) monolayer is dynamically stable. The stability of this monolayer is further confirmed by the MD simulation results, as shown in Fig. 1(c) and (d). The Y-O bond displacement is within 0.18 Å at the simulated temperature of 300 K during the 10 ps MD simulation. The configuration of Y_2O_3 monolayer supercell at the maximum bond displacement (about 0.18 Å) is shown in Fig. 1(e) and (f). It can be seen that only slight distortion is found in Y_2O_3 monolayer at room temperature.

The electronic and dielectric properties of the planar Y_2O_3 (111) monolayer are shown in Fig. 2. From the calculated HSE06 band structure (Fig. 2(a)), both valence band maximum and conduction band mini-mum are located at the Γ point, suggesting a direct band gap of 3.96 eV. This band gap is smaller than that of bulk Y_2O_3 due to different bonding characters. The corresponding total and projected density of states (DOS) are presented in Fig. 2(b), in which the flat valence band maximum is mainly derived from the $2p$ orbital of O atoms, weakly hybridized with $5d$ orbital of Y atoms, forming σ bonds. For the lower valence bands (-1.4 eV$\sim$-0.8 eV), the formation of π bonds is found as p_z orbitals of O atoms and t_{2g} orbitals of Y atoms hybridize to each other, which favors the formation of planar two-dimensional structure.[26] The calculated dielectric function of this planar Y_2O_3 (111) monolayer is presented in Fig. 2(c). The static di-electric constant of the Y_2O_3 (111) monolayer is 1.5. It is noted that only the electronic contributions were included in the calculations. Even taking into account other effects such as ionic and dipolar contributions the calculated dielectric constant of Y_2O_3 (111) monolayer is still smaller than that of Y_2O_3 bulk due to the

reduced thickness and dimensionality.[41]

One possible way for the growth of the Y_2O_3 (111) monolayer is to deposit Y_2O_3 thin films on substrate. Thus, it is crucial to understand the interaction between the planar Y_2O_3 monolayer and the substrate. Next, we examine the stability and interfacial properties of the planar Y_2O_3 (111) monolayer supported on substrates. In this study, graphene is selected as the substrate as Y_2O_3 (111) monolayer has been deposited on graphene.[32] To model the planar Y_2O_3 (111) monolayer/graphene hybrid interface structure, 2.2% tensile strain is applied on the planar Y_2O_3 (111) monolayer to match $3\times3\times1$ graphene supercell, as shown in Fig. 3(a). The small strain reduces the band gap of the planar Y_2O_3 (111) monolayer by about 0.04 eV, but does not change the orbital characters of the valence band and conduction band. The most stable interfacial configuration (see Fig. 3(a)) is such that the Y atom of the planar Y_2O_3 monolayer is directly above the C ring center and O atom is at the bridge site of C-C bond, similar to interfacial configurations of graphene on SiO_2 and Si_3N_4.[9,18] The interface formation energy is minimized through maximizing the potential local bonding. When supported on graphene, the planar Y_2O_3 (111) monolayer becomes more stable and its energy is lowered by 0.46 eV/atom. In the relaxed structure, Y atoms slightly moved out of the Y_2O_3 plane by about 0.05 Å, toward to the graphene plane slightly, resulting in a longer Y-O bond length of 2.11 Å and slightly buckled Y_2O_3 layer, compared with that of free standing planar Y_2O_3 (111) monolayer. The calculated Y-O bond length is close to the experimental result (2.25 Å), but the Y-Y distance (4.17 Å) is much larger.[32] We also study the structural stability of the planar Y_2O_3 (111) monolayer/graphene at high temperature. From the results of our MD simulation of Y_2O_3 (111) monolayer/graphene carried out at 850 *K* shown in Fig. 3(d) and (e), we can see that the Y_2O_3 monolayer remains stable on graphene at this temperature, but its structural distortion is much more pronounced. The maximum displacement of Y-Y distance is about 0.8 Å. This indicates that Y_2O_3 monolayer tends to buckle at high temperature as observed in a recent experiment.[32]

The DFT-D2 optimized distance between graphene and the planar Y_2O_3 (111) monolayer is found to be 2.96 Å, which is at the boundary between chemical adsorption and physical adsorption ($\sim$3 Å), but far beyond the covalent bonding range of 1.44 Å for C-O bond and 2.4 Å for C-Y bond, respectively. To further investigate the nature of interfacial bonding, electron localization function (ELF) was calculated.[45] Figure. 3(c) shows the ELF in the (110) plane of this stable interfacial configuration. No covalent bonding can be found at the interface between graphene and the planar Y_2O_3 (111) monolayer. To estimate interfacial interaction strength, we calculated the binding energy which is defined as:

$$E_b = E_G + E_{Y_2O_3} - E_{G+Y_2O_3}, \tag{1}$$

where E_G, $E_{Y_2O_3}$, and $E_{G+Y_2O_3}$ are total energies of the isolated graphene, isolated Y_2O_3 slab, and combined graphene and Y_2O_3 (111) monolayer hybrid structure, respectively. The calculated binding energy for this interface is 42 meV per C atom, which is within the range of physical adsorption (10 meV$\sim$100 meV), and suggests a weak interaction between graphene and the planar Y_2O_3 (111) monolayer. This weak interaction is also confirmed by a slight interfacial charge transfer. As shown in Fig. 3(b), due to the presence of the planar Y_2O_3 (111) monolayer, inhomogeneous charge redistribution is found within the graphene layer, but the contribution from Y_2O_3 is very small. Bader charge analysis[46] shows only 0.003 excess electron per C atom in graphene.

The electronic properties of the planar Y_2O_3 monolayer on graphene are shown in Fig. 4. From the DFT-D2 calculated band structure (Fig. 4(a)), it is noted that the conduction band minimum that is derived from C p_z orbital is about 0.015 eV below the Fermi energy, indicating that graphene is slightly n-doped. We also found that a gap of about 0.21 eV is opened in graphene. Figure 4(b) is the calculated projected density of states for Y_2O_3 (111) monolayer on graphene. Hybridization is found between O p_z and C p_z states near the Fermi energy, as well as Y t_{2g} and C p_z states. In the energy range of -1 eV to -2 eV, the hybridization between O p_z and C p_z, and also between C p_z and Y e_g states are more profound. These orbital hybridizations are further confirmed by the partial charge density at the lower Dirac cone of graphene, where the dominant contribution is from C p_z orbital, but minor contribution from O atoms is noticeable also, as shown in Fig. 4(c). The origins of gap opening in graphene after integration with the Y_2O_3 (111) monolayer can be ascribed to structural deformation, or interfacial interaction with Y_2O_3, or both. To determine which of the above factors play a dominate role, we calculated the band structure of the isolated deformed graphene by removing the planar Y_2O_3 (111) monolayer. The results show that this deformed graphene does not affect its band structure. Thus, the gap opening in graphene is due to interfacial interaction by the presence of the planar Y_2O_3 (111) monolayer.

A number of factors could affect the interfacial interaction between graphene and the planar Y_2O_3 monolayer, including the interfacial vdW interaction, charge transfer, orbital hybridization, and electrostatic potential interaction. The interfacial charge transfer is not expected important for determining the interaction because only about 0.003 electrons per C atom were transferred from Y_2O_3 to graphene. The effect of vdW interactions can be estimated by comparing the structural and electronic properties of Y_2O_3 monolayer on

graphene with and without the vdW correction. Our calculations show that without vdW correction the GGA optimized spacing between graphene and the Y_2O_3 monolayer is significantly increased to 3.6 Å. The band structure of graphene (see Fig. 4(d)) is similar to that of free standing graphene, but with a small gap of 0.04 eV that is due to electrostatic energy difference in graphene AB lattices caused by Y_2O_3 at this GGA optimized interfacial spacing distance. This shows that vdW interaction play a very important role in determining the spacing distance between graphene and the planar Y_2O_3 monolayer. Moreover, the effect of vdW interactions on the electronic properties can be seen from the difference between band structures calculated with and without vdW correction. The band structure in Fig. 4(a) is calculated using DFT-D2 method, which is force correction that only affects the structural configuration. In comparison, the band structure in Fig. 4(e) is calculated using vdW-DF method with optB88-vdW functional[38], which is a self consistent vdW correction method and vdW interaction effect is included in the band structure calculation. It is noted that these two band structures are nearly identical. These suggest that vdW interaction bounds Y_2O_3 monolayer with graphene, but it does not significantly influence its electronic properties.[33,47,48] In addition, for the 0.21 eV gap in graphene, about 0.08 eV is ascribed to interfacial electrostatic potential interaction because the electrostatic potential energy difference in graphene AB lattices is about 0.08 eV at the presence of Y_2O_3 monolayer.[10,12,48]. The rest contribution should mainly originate from the orbital hybridization as the interfacial charge transfer is very weak and the interfacial vdW interaction does not affect electronic structure. Therefore, orbital hybridization plays an important role in determining electronic properties at the interface of Y_2O_3 monolayer/graphene. It is noted that a similar phenomenon has been found at the interface between graphene and Ni, where the adsorption is a typical physisorption, but the electronic structure is mainly determined by orbital hybridization.[49] We also studied the interfacial properties of buckled Y_2O_3 monolayer on $(2\times2\times1)$graphene. The optimized lattice constant is 5.14 Å, and the calculated Y-Y and Y-O length is about 2.96 and 1.96 Å, respectively. It is also noted that when supported on graphene, the buckled Y_2O_3 (111) monolayer became much more stable as its energy is dramatically lowered (about 2.7 eV per Y_2O_3 unit). The Dirac cone of graphene is still preserved at the presence of buckled Y_2O_3 (see Fig. 5(a) and (b)), but is shifted about 1.1 eV below Fermi energy, in agreement with experimental observation.[32]

Another possible way to realize the planar Y_2O_3 (111) monolayer is to oxidize yttrium (Y) (0001) surface directly. Thus, we further study the interface of the planar Y_2O_3 (111) monolayer on Y (0001) substrate. In the most stable structure, the O atoms of the Y_2O_3 (111) monolayer are on the top of Y atom of yttrium (001) substrate. The interaction between the Y_2O_3 monolayer and Y is much stronger compared

to that between the planar Y_2O_3 monolayer and graphene, as the interfacial binding energy is as high as 300 meV and interfacial Y-O bond is formed with a bond length of 2.25 Å, close to the Y-O bonds in bulk Y_2O_3. The strong interaction also leads to a significant outward relaxation (0.4 Å) of O atoms in Y_2O_3 (111) monolayer towards the Y substrate, turning the planar monolayer into a buckled structure. For the two possible methods to grow the Y_2O_3 monolayer, the direct oxidation method, due to strong interaction between Y_2O_3 and Y substrate as mentioned above, the grown Y_2O_3 layers tend to be buckled. This is also applied to the physical deposition of Y_2O_3 on a substrate that has strong interaction with Y_2O_3 layers. In both cases, even though a distorted Y_2O_3 monolayer can be grown, it is difficult to be exfoliated or transferred for further functionization as the bind energy between them is large. Thus, a more promising method to grow Y_2O_3 monolayer is through physical deposition process on a substrate with weak interfacial interaction like the planar Y_2O_3 monolayer on graphene.

4 Conclusions

In conclusion, the results of our first-principles calculations predict a stable Y_2O_3 (111) monolayer, which has a direct band gap 3.96 eV. The Y_2O_3 (111) monolayer can be further stabilized by depositing it on graphene. The weak interaction between the Y_2O_3 (111) monolayer and graphene indicates that the inert graphene surface is an excellent substrate to grow an Y_2O_3 (111) two-dimensional monolayer. This growth strategy might be applied to grow other similar high-κ dielectric monolayer on the chemical inert surface. Due to similar surface chemical nature among graphene and other two-dimensional materials such as MoS_2, or black phosphene, our results may shed light on understanding interfacial interaction between two-dimensional materials and other extremely thin high-k oxide films.

5 Acknowledgement

6   Graphics and tables
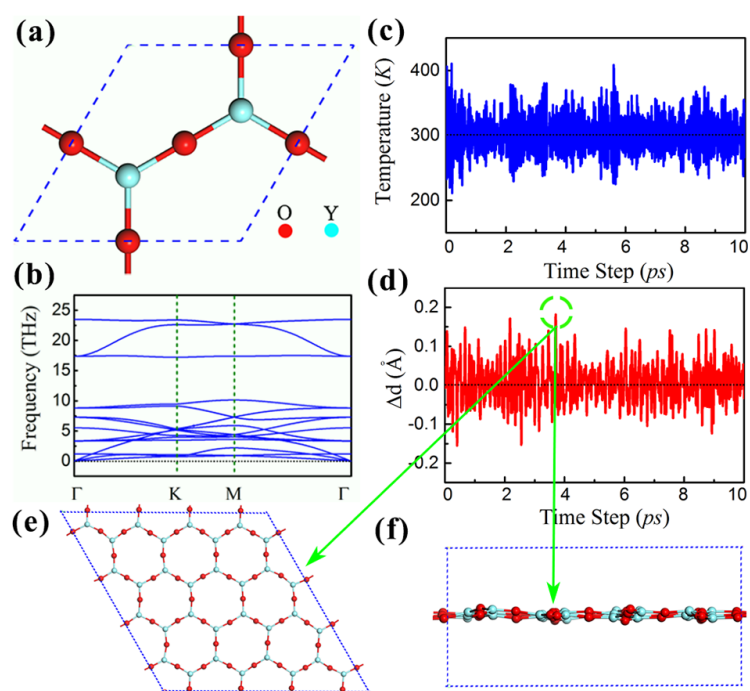
Fig. 1 (a) Top view of the planar Y_2O_3 (111) monolayer. (b) Phonon dispersion of the planar Y_2O_3 (111) monolayer. The temperature evolution (c) and the evolution of Y-O bond (d) during the 10 ps MD simulation at room temperature, in which the bond displacement Δd is defined as the difference between the Y-O bond length in MD simulations (d) and its equilibrium bond length (d_0). The top view (e) and side view (f) for the Y_2O_3 (111) monolayer with the maximum bond displacement during 10 ps the MD simulation.
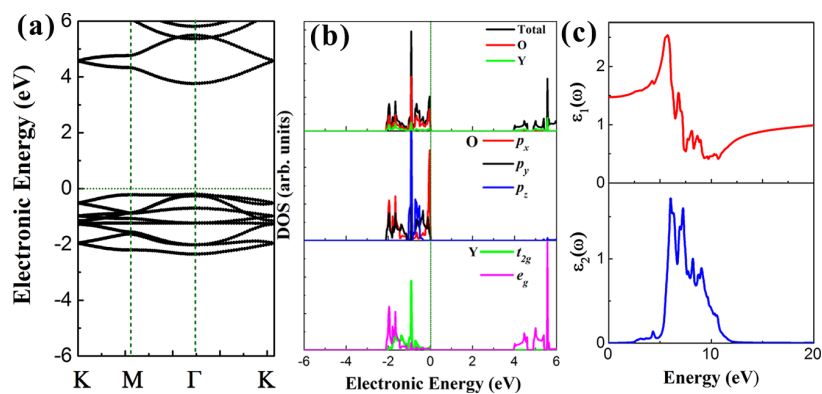
Fig. 2 (a) Band structure (b) Total and projected DOS of the planar Y_2O_3 (111) monolayer. (c) Dielectric function of the Y_2O_3 monolayer. The navy dotted line denotes the Fermi level.
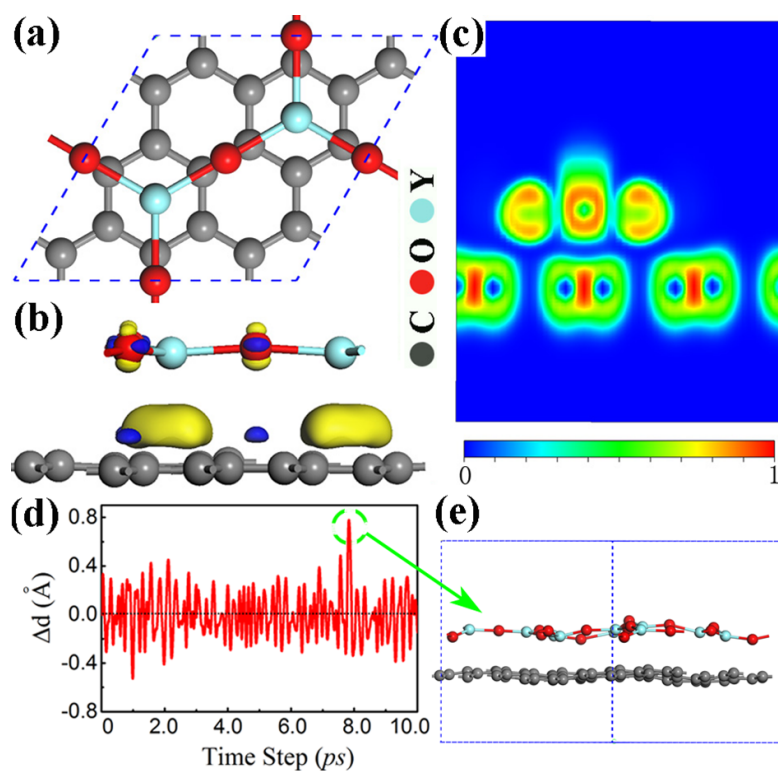
Fig. 3 (a) Top view of the planar Y_2O_3 (111) monolayer on the ($3\times3\times1$) graphene. (b) Side view of charge density difference between the Y_2O_3 (111) monolayer and graphene, where the charge density difference ($\Delta\rho$) is defined by $\Delta\rho=\rho_{(G+Y_2O_3)}-\rho_G-\rho_{Y_2O_3}$, and visualized with an isosurface value of 1.0×1.0^{-3} eV/Å^3. Yellow color denotes excess charge density and blue color denotes depleted charge density. (c) Contour plot of the ELF for the planar Y_2O_3 (111) monolayer on the graphene along (110) plane. (d) The evolution of Y-Y distance for the Y_2O_3 (111) monolayer on the graphene during 10 *ps* MD steps at the temperature of 850 *K*. (e) The side view of the structural configuration with the maximum displacement of Y-Y distance during the MD simulation.
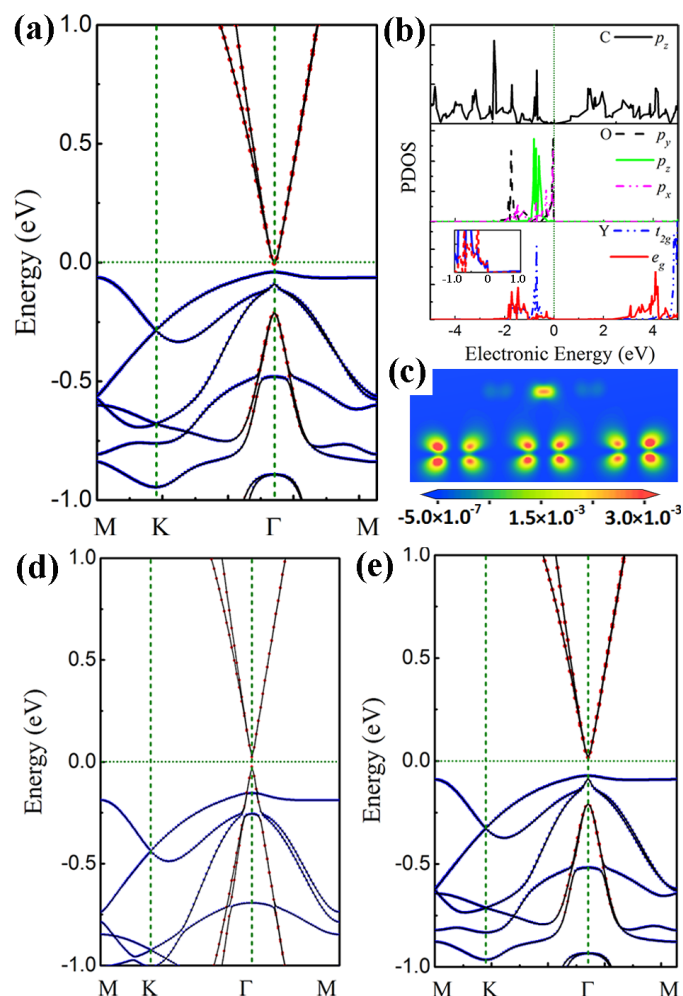
Fig. 4 Electronic structure of Y_2O_3 (111) monolayer on graphene. (a) Orbital projected band structure for the planar Y_2O_3 (111) monolayer on the (3×3×1) graphene at the DFT-D2 optimized spacing distance of 2.96 Å, in which red solid dots and blue solid lattices denote the contribution from C p_z and O p orbitals, respectively. (b) Projected density of states (PDOS) of C atom in graphene, and its nearest O and Y atom in Y_2O_3. The inset is zoomed PDOS of Y atoms near Fermi level. (c) Contour plot of partial charge density for the top π orbital in graphene. (d) GGA Band structure (without vdW correction) of planar Y_2O_3 (111) monolayer on the graphene at the GGA optimized interfacial spacing of 3.60 Å. (e) vdw-DF (optB88 functionals) band structure of planar Y_2O_3 (111) monolayer on the graphene at the vdW-DF optimized distance of 3.06 Å.
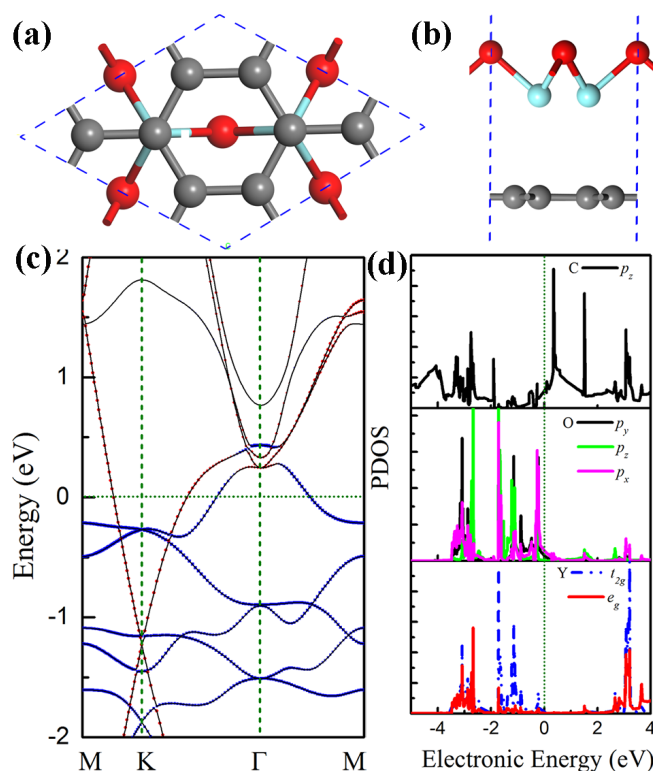
Fig. 5 The top (a) and side (b) view of the atomic structure for Y_2O_3 (111) monolayer on ($2\times2\times1$) graphene. The corresponding band structure (c) and PDOSs (d).

References

1 G. D. Wilk, R. M. Wallace, and J. Anthony, *J. Appl. Phys.,* 2001, **89**, 5243-5275.

2 J. Robertson, *Rep. Prog. Phys.,* 2006, **69**, 327-396.

3 K. Novoselov , D. Jiang, F. Schedin, T. Booth, V. Khotkevich, S. Morozov, and A. Geim, *Proc. Natl. Acad. Sci. USA,* 2005, **102**, 10451-10453.

4 A. K. Geim and K. S. Novoselov, *Nat. Mater.,* 2007, **6**, 183-191.

5 A. C. Neto, F. Guinea, N. Peres, K. S. Novoselov, and A. K. Geim, *Rev. Mod. Phys.,* 2009, **81**, 109-162.

6 K. S. Novoselov , V. I. Falko, L. Colombo, P. R. Gellert, M. G. Schwab, and K. Kim, *Nature,* 2012, **490**, 192-200.

7 X. Du, I. Skachko, A. Barker, and E. Y. Andrei, *Nat. Nanotech.,* 2008, **3**, 491-495.

8 L. Liao,J. Bai, Y. Qu, Y.-C. Lin, Y. Li, Y. Huang, and X. Duan, *Proc. Natl. Acad. Sci. USA,* 2010, **107**, 6711-6715.

9 Y.-J. Kang, J. Kang, and K. Chang, *Phys. Rev. B,* 2008, **78**, 115404.

10 N. T. Cuong, M. Otani, and S. Okada, *Phys. Rev. Lett.,* 2011, **106**, 106801.

11 K. Kamiya, N. Umezawa, and S. Okada, *Phys. Rev. B,* 2011, **83**, 153413.

12 B. Huang, Q. Xu, and S.-H. Wei, *Phys. Rev. B,* 2011, **84**, 155406.

13 P. Havu, M. Ijäs, and A. Harju, *Phys. Rev. B,* 2011, **84**, 205423.

14 W. Scopel, A. Fazzio, R. Miwa, and T. Schmidt, Phys. Rev. B, 2013, **87**, 165307-165312.

15 L. Liao, J. Bai, R. Cheng, Y.-C. Lin, S. Jiang, Y. Huang, and X. Duan, *Nano Lett.,* 2011, **10**, 1917-1921.

16 L. Liao, J. Bai, Y.-C. Lin, Y. Qu, Y. Huang, and X. Duan, *Adv. Mater.,* 2010, **22**, 1941-1945.

17 W. Zhu, D. Neumayer, V. Perebeinos, and P. Avouris, *Nano Lett.,* 2010, **10**, 3572-3579.

18 M. Yang, J. Chai, Y. Wang, S. Wang, and Y. Feng, *J. Phys. Chem. C,* 2012, **116**, 22315-22318.

19 M. Yang, C. Zhang, S. Wang, Y. Feng, and Ariando, *AIP Adv.,* 2011, **1**, 032111-032118.

20 L. Wang, X. Chen, Y. Wang, Z. Wu, W. Li, Y. Han, M. Zhang, Y. He, C. Zhu, K. K. Fung et al., *Nanoscale,* 2013, **5**, 1116-1120.

21 Z. Wang , H. Xu, Z. Zhang, S. Wang, L. Ding, Q. Zeng, L. Yang, T. Pei, X. Liang, and M. Gao, *Nano Lett.,* 2010, **10**, 2024-2030.

22 A. Kara, H. Enriquez, A. P. Seitsonen, L. L. Y. Voon, S. Vizzini, B. Aufray, and H. Oughaddou, *Surf. Sci. Rep.,* 2012, **67**, 1-18.

23 L. Li, Y. Yu, G. J. Ye, Q. Ge, X. Ou, H. Wu, D. Feng, X. H. Chen, and Y. Zhang, *Nat. Nanotech.,* 2012, **9**, 372-377.

24 H. Liu, A. T. Neal, Z. Zhu, Z. Luo, X. Xu, D. Tomanek, and P. D. Ye, *ACS nano,* 2014, **8**, 4033-4041.

25 M. Topsakal, S. Cahangirov, E. Bekaroglu, and S. Ciraci, *Phys. Rev. B,* 2009, **80**, 235119.

26 H. Zhuang, A. K. Sing, and R. G. Hennig, *Phys. Rev. B,* 2013, **87**, 165415.

27 H. Sahin, S. Cahangirov, M. Topsakal, E. Bekaroglu, E. Akturk, R. T. Senger, and S. Ciraci, *Phys. Rev. B,* 2009, **80**, 155453.

28 C. Ataca, H. Sahin, and S. Ciraci, *J. Phys. Chem. C,* 2012, **116**, 8983-8999.

29 C. Bacaksiz, H. Sahin, H. D. Ozaydin, S. Horzum, R. T. Senger, and F. M. Peeters, *Phys. Rev. B,* 2015, **91**, 085430.

30 Y. Aierken, H. Sahin, F. Iyikanat, S. Horzum, A. Suslu, B. Chen, R. T. Senger, S. Tongay, and F. M. Peeters, *Phys. Rev. B,* 2015, **91**, 245413.

31 D. Löffler, J. J. Uhlrich, M. Baron, B. Yang, X. Yu, L. Lichtenstein, L. Heinke, C. Büchner, M. Heyde, S. Shaikhutdinov et al., *Phys. Rev. Lett.,* 2010, **105**, 146104.

32 R. Addou, A. Dahal, and M. Batzill, *Nat. Nanotech.,* 2013, **8**, 41-45.

33 G. Giovannetti, P. A. Khomyakov, G. Brocks, P. J. Kelly, and J. van den Brink, *Phys. Rev. B, 2007,* **76**, 073103.

34 G. Kresse and J. Hafner, *Phys. Rev. B,* 1993, **47**, 558.

35 G. Kresse and J. Hafner, *Phys. Rev. B,* 1993, **48**, 13115.

36 P. E. Blöchl, *Phys. Rev. B,* 1994, **50**, 17953.

37 X. Wu, M. Vargas, S. Nayak, V. Lotrich, and G. Scoles, *J. Chem. Phys.,* 2001, **115**, 8748-8757.

38 J. Klimeš, D. R. Bowler, and A. Michaelides, *Phys. Rev. B,* 2011, **83**, 195131.

39 J. Heyd, G. E. Scuseria, and M. Ernzerhof, *J. Chem. Phys.,* 2003, **118**, 8207-8215.

40 A. Togo, F. Oba, and I. Tanaka, *Phys. Rev. B,* 2008, **78**, 134106.

41 Y.-N. Xu, Z.-Q. Gu, and W. Ching, *Phys. Rev. B,* 1997, **56**, 14993.

42 G. Henkelman, A. Arnaldsson, and H. Jónsson, *Comput. Mater. Sci.,* 2006, **36**, 254.

43 X. J. Liu, et al., *Chem. Rev.* 2015, **115**, 6746.

44 X.-G. Wang, A. Chaka, and M. Scheffler, *Phys. Rev. Lett.,* 2000, **84**, 3650.

45 A. D. Becke and K. E. Edgecombe, *J. Chem. Phys.,* 1990, **92**, 5397-5403.

46 G. Henkelman, A. Arnaldsson, and H. Jónsson, *Comput. Mater. Sci.,* 2006, **36**, 354-360.

47 C. R. Dean , A. F. Young, I. Meric, C. Lee, L. Wang, S. Sorgenfrei, K. Watanabe, T. Taniguchi, P. Kim, K. L. Shepard et al., *Nat. Nanotech.,* 2010, **5**, 722-726.

48 E. Kan, H. Ren, F. Wu, Z. Li, R. Lu, C. Xiao, K. Deng, and J. Yang, *J. Phys. Chem.,* 2012, **116**, 3142-3146.

49 F. Mittendorfer, A. Garhofer, J. Redinger, J. Klimeš, J. Harl, and G. Kress, *Phys. Rev. B,* 2011, **84**, 201401(R).